RSC Advances

PAPER

View Article Online
View Journal | View Issue

Cite this: *RSC Adv.*, 2021, **11**, 23036

Clean water generation through a multifunctional activated carbon-TiO_2 interfacial solar distillation system†

Kuan-Yu Chen,[a] Webber Wei-Po Lai,[ab] Hui-Ju Wang,[a] Cheng-Chieh Lin,[ce] Chun-Wei Chen[cd] and Angela Yu-Chen Lin*[ac]

Solar distillation is emerging as an environmentally friendly and energy-effective technology for clean water generation. However, bulk water heating and the possibly complex composition of water matrices of source water could undermine the system efficacy. In this study, an interfacial evaporation device consisting of activated carbon combined with P25 TiO_2 as the top layer and polyethylene foam as the bottom layer (AC-P25/foam device) was established. With the excellent optical absorbance of AC and the heat localization effect contributed by the PE foam, the evaporation rate (r_{evp}) of the device (r_{evp} = 2.1 kg m^{-2} h^{-1}) was improved by 209% and 71% compared with that of the water-only (r_{evp} = 0.68 kg m^{-2} h^{-1}) and conventional evaporation (*i.e.*, submerged AC-P25) systems (r_{evp} = 1.23 kg m^{-2} h^{-1}), respectively. The reusability test showed the stable evaporation performance of AC-P25/foam within 7 cycles; this interfacial evaporation was also found to be less affected by suspended solids in water due to a reduction in the influence of light scattering. The AC-P25/foam device not only possessed photothermal ability for water distillation but was also able to prevent enrichment of volatile organic compounds (*i.e.*, phenol) with ~95% removal efficiency through adsorption and photocatalytic reactions under illumination. Additionally, an outdoor solar distillation test performed with synthetic saline water demonstrated the desalination ability of the AC-P25/foam device, with the concentrations of all ions in the distilled water ≤3.5 mg L^{-1}, far below the drinking water guideline value provided by the World Health Organization. The materials of the AC-P25/foam photothermal device are readily available and easily fabricated, showing the practical feasibility of this device for clean water generation.

Received 19th March 2021
Accepted 22nd June 2021

DOI: 10.1039/d1ra02185k

rsc.li/rsc-advances

1. Introduction

Water is essential to every living creature on Earth, and the production of clean water is also the foundation of human civilization. Due to climate change and the rapid development of human society, the quantity and quality of freshwater resources have deteriorated, leading to water scarcity and water shortage issues. Therefore, using alternative water resources such as seawater or wastewater as water sources is necessary.

Regarding desalination and water reuse, membrane-based technologies are always major solutions. Although the ability of membranes to generate clean water has been proven, membrane-based technologies often suffer from scaling, fouling, and high power consumption, thus resulting in problems related to maintenance and operation,[1] which may be obstructive for development in areas lacking energy infrastructure. Solar distillation is considered a promising approach for generating clean water through an evaporation–condensation process, and the process utilizes sunlight, which is a renewable and nearly infinite energy resource.[2] A typical conventional solar distillation system is composed of a photothermal layer at the bottom and an inclined surface to condense water vapor.[3] Incident sunlight is absorbed by the source water and the photothermal layer; the absorbed light is then converted to thermal energy to heat the entire body of water to generate solar steam.

Although solar distillation has been in use for a long time, the efficiencies of conventional solar distillation are often limited due to the poor solar absorption of water, bulk water heating and susceptibility to water turbidity.[4–8] To overcome the potential problems of traditional solar distillation, the concept

[a]*Graduate Institute of Environmental Engineering, National Taiwan University, 71-Chou-shan Road, Taipei 106, Taiwan. E-mail: yuchenlin@ntu.edu.tw; Tel: +886-2-3366-4386*

[b]*Department of Environmental Science and Engineering, Tunghai University, Taichung 407, Taiwan*

[c]*International Graduate Program of Molecular Science and Technology, National Taiwan University (NTU-MST), Taipei 106, Taiwan*

[d]*Department of Materials Science and Engineering, National Taiwan University, No. 1, Sec. 4, Roosevelt Rd., Taipei 106, Taiwan*

[e]*Molecular Science and Technology Program, Taiwan International Graduate Program, Academia Sinica, Taiwan*

† Electronic supplementary information (ESI) available. See DOI: 10.1039/d1ra02185k

of heat localization was first proposed by Ghasemi *et al.*[9] By placing a photothermal material on top of a thermal insulation layer, the thermal energy generated from incident sunlight can be localized at the air–water interface; the heat localization effect induced by the thermal insulation layer makes the evaporation of water more efficient.[10] In the last few years, many studies have utilized this photothermal technique for solar distillation; in these currently published studies, to enhance light absorbance ability, the improvement in the architectural design of solar distillation systems has been investigated. For instance, Zhu *et al.* noted that the design of a photothermal material with a three-dimensional architecture can reclaim light reflections, further enhancing light absorption.[11] Another focus for achieving promising solar steam generation is optimization of the photothermal material selection/fabrication. Among photothermal materials, both plasmonic metal nanoparticles and carbon-based materials are commonly used. Plasmonic nanoparticles can absorb solar energy owing to their localized surface plasmon resonance effect, further leading to light-to-heat conversion.[12] However, these materials have the disadvantage of exhibiting relatively narrow band absorption (limited mainly to the visible light range);[13] additionally, plasmonic nanoparticles (*e.g.*, gold, silver and palladium) are usually expensive, making them unideal for large-scale application.[14] Instead, carbon-based materials not only have the merits of low cost and high accessibility but also can exhibit high-efficiency light absorption across the full solar spectrum. Through lattice vibrations in carbon materials, the incident photon energy can be converted into heat,[15] so they are generally considered to be superior light absorbers exhibiting good water evaporation efficiency.[16] Li *et al.* recently utilized a commercially activated carbon fiber material for efficient solar steam generation.[13]

Despite continuous evolvement, the main weakness of solar distillation still exists when water contaminated with volatile organic compounds (VOCs), such as industrial effluents and groundwater, is used as the source water. Although chemicals with high boiling points can be easily separated during solar distillation, VOCs with low boiling points are vaporized simultaneously through water evaporation. Subsequently, VOCs in the vapor phase may even further condense with distilled water at the same time, leading to VOC enrichment in the distillate and thus polluting the clean water generated, as noted by Wang *et al.*[17] In fact, it has been demonstrated that by using phenol solutions (10–100 mg L^{-1}) as the source water in solar distillation, 50%–280% more phenol was detected in the distilled water than in the original phenol solutions,[18] indicating possible pollution of distilled water by VOCs. However, compared with other high-boiling-point contaminants (*e.g.*, dye pollutants) studied in current published works,[19–21] the influence of VOCs on solar distillation has rarely been studied, which may be of greater concern in the solar distillation process. To the best of our knowledge, only two studies[22,23] have recently explored the influence of VOCs (using phenol solutions as source water) on clean water generation through solar-driven water evaporation. Shi *et al.* introduced an oxidant-based method into a solar distillation process that showed a high (~98.2%) VOC removal efficiency.[22] However, the requirement of adding an H_2O_2 oxidant significantly increases the cost; this method is also slightly inconvenient for practical use. Song *et al.* proposed a nanofibrous membrane material that can effectively intercept VOCs *in situ* in the evaporation process,[23] while the fabrication process includes complex stages.

To achieve the goal of clean water harvesting *via* synchronous solar-driven water evaporation and VOC removal, an interfacial evaporation device that is easily fabricated and combined with readily available materials, including activated carbon (AC), P25 TiO_2 and polyethylene foam (PE foam) (denoted AC-P25/foam), was proposed in this work. AC serves as the main photothermal material, exhibiting excellent optical absorption; additionally, the adsorption ability of AC enables the removal of VOCs transported to the surface of the device. P25 TiO_2 is incorporated into the AC due to its photocatalytic activity to further degrade the VOCs on the device surface. PE foam is expected to localize the thermal energy generated at the device surface due to its low thermal conductivity ($k = 0.026$ W m^{-1} K^{-1}).[24] The advantages of these materials make the AC-P25/foam device a promising solar-driven evaporator. The specific aims of this work are to (i) study the steam generation performance by utilizing the AC-P25/foam interfacial evaporation devices and explore the heat localization phenomena of the system, (ii) examine the reusability of the AC-P25/foam device and study the effect of suspended solids on steam generation, and (iii) investigate the effect of different source water matrices, including VOC-containing water and synthetic saline water, on the solar distillation process. By utilizing the interfacial evaporation system, a high steam generation efficiency and successful prevention of VOC enrichment without the additional use of chemical reagents were achieved. High distilled water productivity and acceptable water quality both indicate the potential of interfacial evaporation in clean water generation.

2. Materials and methods

A flowchart of the experimental methodology of this study is provided in the ESI (Fig. S1†); the chemicals/materials used, experimental device setup and procedure and sample characterization and analysis are described in detail as follows.

2.1 Materials

Commercial TiO_2 (P25) was purchased from Degussa (Germany). Untreated granular AC (20–60 mesh), 1-methyl-2-pyrrolidinone (NMP, 99.5%), sea salt and kaolinite were purchased from Sigma-Aldrich (St Louis, MO, USA). The physicochemical properties of AC, P25 TiO_2 and PE foam are provided in the Supplementary Information (Table S1†). Immobilon-P PVDF membrane, phenol (≥99.0%) and acetonitrile (HPLC grade, ≥99.9%) were purchased from Merck (Darmstadt, Germany). Lens tissues (11.2 × 21.3 cm) were purchased from Kimtech (USA). Sodium chloride (≥99.5%) was purchased from Nacalai Tesque (Japan). Ferric ion solution and mercuric thiocyanate solution were purchased from Hach (USA). Flake graphite (100 mesh) was purchased from Uni-Region Bio-tech (Taiwan). Deionized water (DI water) produced

by a Milli-Q system (Millipore Co., MA, USA) with a conductance of 18.2 MΩ cm was used in all experiments. A stock solution of phenol (500 mg L^{-1}) was prepared in DI water and stored at 4 °C for a maximum of 1 month.

2.2 Construction of interfacial evaporation devices

Two types of materials were used as the photothermal layer, AC blended with TiO_2 (AC-P25) and flake graphite. AC was first manually ground to smaller fragments before the fabrication process. A 30 mg PVDF membrane was dissolved in 2 mL of NMP. Thereafter, 220 mg of AC was added to the solution followed by vortex shaking for 30 min. Then, 50 mg of TiO_2 was added to the AC dispersion followed by vortex shaking for 30 min and sonication for 1 h to obtain a uniform dispersion. Finally, AC-P25 was pasted into a circular shape with a diameter of 3.5 cm on lens tissue using the doctor blade technique; this technique is considered to be a fast and non-energy-consuming procedure for uniformly and reproducibly producing a thin coated layer with a designated film thickness.[25,26] Lens tissue loaded with AC-P25 was then dried in an oven at 50 °C. To fabricate graphite-loaded lens tissue, 270 mg of graphite was substituted for AC and TiO_2. Lens tissue samples loaded with different photothermal materials were placed on PE foam (2 cm thickness) to construct the interfacial evaporation devices (*i.e.*, AC-P25/foam, graphite/foam). PE foam was chosen due to its low thermal conductivity. Four strips of lens tissue with lengths of 2 cm and widths of 1 cm served as water transportation pathways. PE foam wrapped with pristine lens tissue (lens tissue/foam) was also prepared for the control experiment. Pictures of AC-P25/foam and graphite/foam are presented in Fig. 1(a) and (b).

2.3 Characterization

The absorption spectra of AC, AC-P25 and graphite were measured in a wavelength range from 300 to 2000 nm using a Cary 5000 ultraviolet-visible-near infrared (UV-vis-NIR) spectrophotometer (Agilent Technologies, Santa Clara, CA, USA). The morphologies of different lens tissue samples were characterized by field emission scanning electron microscopy (FESEM, FEI NOVA NanoSEM 230, USA). Energy dispersive spectrometry (EDS) analysis was also conducted using an X-Max EDS detector (Oxford Instruments, Oxford, UK) coupled to the FESEM instrument to check the elemental compositions of certain regions on the lens tissue samples.

2.4 Steam generation test

To thoroughly investigate the effectiveness of interfacial evaporation, steam generation tests under different conditions were performed, including using AC-P25/foam, graphite/foam, lens tissue/foam, AC-P25 submerged at the bottom (submerged AC-P25), and only water. Forty milliliters of DI water was poured into a 50 mL beaker, and the beaker was placed in a foam container to reduce the heat exchange with the surroundings. The system with or without a steam generation device was then illuminated with a Suntest CPS solar simulator (Atlas, Chicago, IL, USA) equipped with a 1.5 kW xenon arc lamp for 45 min (a photo of the solar simulator is provided in Fig. S2†). An LP 471 PYRA 02.5 pyranometer equipped with an HD2102.2 datalogger (Delta OHM, Padova, Italy) was utilized for measurement of the

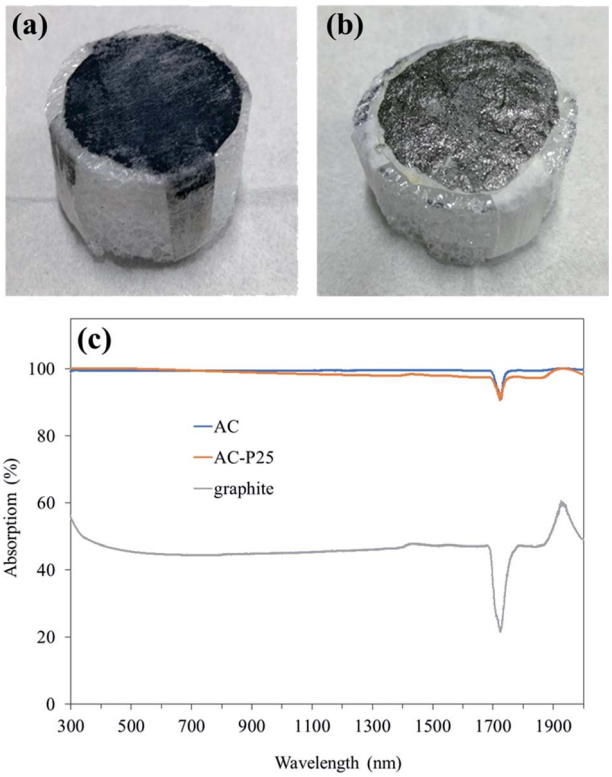

Fig. 1 Pictures of (a) AC-P25/foam and (b) graphite/foam. (c) UV-vis-NIR absorption spectra of the different photothermal layers.

total flux density of radiation (ranging between 300 and 3000 nm). In the solar simulator, the total light intensity from 300–3000 nm was measured as 998 W m^{-2}, which is approximately equivalent to the light intensity of one sun (1000 W m^{-2}). The weight change of the system was measured every 5 min by an electronic balance (AL104, Mettler Toledo, Greifensee, Switzerland); the accuracy of the balance was 0.0001 g. After the steam generation experiments, the chamber door of the solar simulator was opened, and the temperature distribution of the solution was immediately recorded using an FLIR E5 IR camera (FLIR Systems, Inc., Wilsonville, OR, USA).

2.5 Clean water generation by a solar still system

Clean water generation through solar distillation was demonstrated with a self-designed solar still system. The system was fabricated by TOCHANCE (Taoyuan, Taiwan) using quartz and was composed of three parts: a hemispherical top cover (inner diameter = 156 mm, height = 28 mm), an outer bowl (inner diameter = 155 mm, height = 134.55 mm) and an inner bowl (inner diameter = 95 mm, height = 85 mm). The pictures of the solar still system are presented in the ESI (Fig. S3†).

The ability of AC-P25/foam to prevent phenol enrichment was studied. A solution containing 10 mg L^{-1} phenol was prepared to simulate VOC-polluted water. The experimental setup and illumination conditions have been described above. After irradiation, the distilled water in the outer bowl was collected, and the phenol concentrations in the initial phenol solution, the solution after solar distillation and distilled water were analyzed.

On the other hand, the desalination ability of AC-P25/foam was also assessed using synthetic saline water (3.5 wt% sea salt dissolved in DI water) as the source water because the concentration of salt in real seawater (*i.e.*, salinity) is approximately 3.5 wt%. The sea salt was harvested from an ocean deposit, and thus, the composition of the solution very closely resembled the composition of seawater. Four pieces of AC-P25/foam were placed on the surface of 150 mL of synthetic saline water within the inner bowl of the solar still and irradiated under the same illumination conditions used in the steam generation test for 6 h. After irradiation, the distilled water in the outer bowl was collected, and the ion concentrations (Cl^-, Na^+, Mg^{2+}, Ca^{2+} and K^+) in the initial saline water and distilled water were measured. The detailed analyses of phenol and the ions are described in Section 2.6.

2.6 Analysis

The phenol concentration was determined *via* high-performance liquid chromatography coupled with a diode-array detector (HPLC-DAD; Agilent 1200 module, Agilent Technologies, Santa Clara, CA, USA) and an Eclipse C_{18} column (150 × 4.6 mm, 5 μm). The mobile phase was composed of 40% acetonitrile and 60% DI water and flowed under isocratic operation at a flow rate of 1 mL min^{-1}. Before analysis, the DI water utilized as the mobile phase was filtered through a 0.2 μm cellulose acetate membrane. The detection wavelength for phenol was 270 nm (reference wavelength: 360 nm); the injection volume was 100 μL. Phenol removal was characterized by the C/C_{-90} value, where C is the concentration of phenol at time t and C_{-90} is the initial phenol concentration. The concentrations of Cl^- in the original synthetic saline water and distilled water were measured using the mercuric thiocyanate method and analyzed with a DR 6000 UV-vis spectrophotometer (Hach; Loveland, CO, USA) (the detailed analytical procedure is described in the ESI (Text S1†)); Na^+, Mg^{2+}, Ca^{2+} and K^+ concentrations were analyzed using inductively coupled plasma optical emission spectrometry (ICP-OES, Agilent 700 series, Santa Clara, CA, USA).

3. Results and discussion

3.1 Characterization

UV-vis absorption spectra of the different materials were obtained to determine the possible photothermal material suitable for solar steam generation. With a higher optical absorption, more light is absorbed by the material, thus increasing the solar energy that can be harnessed. The UV-vis-NIR absorption spectra of AC, AC-P25 and graphite are shown in Fig. 1(c). Compared with graphite, materials containing AC absorbed more light in the UV-vis-NIR regions, suggesting that AC-containing materials are better photothermal materials. The SEM image and EDS spectrum of a lens tissue sample loaded with AC-P25 also supported the existence of P25 in the material. The surface of lens tissue fiber became rather rough after being loaded with AC (Fig. 2(a)–(c)). The existence of P25 in the photothermal layer (*i.e.*, AC-P25) was further verified by the EDS spectrum (Fig. 2(d)). Moreover, EDS elemental mapping (Ti element) of the AC-P25 image (Fig. 2(e)) showed that Ti elements were uniformly distributed on the surface of the material, indicating successful incorporation of P25 in the photothermal material.

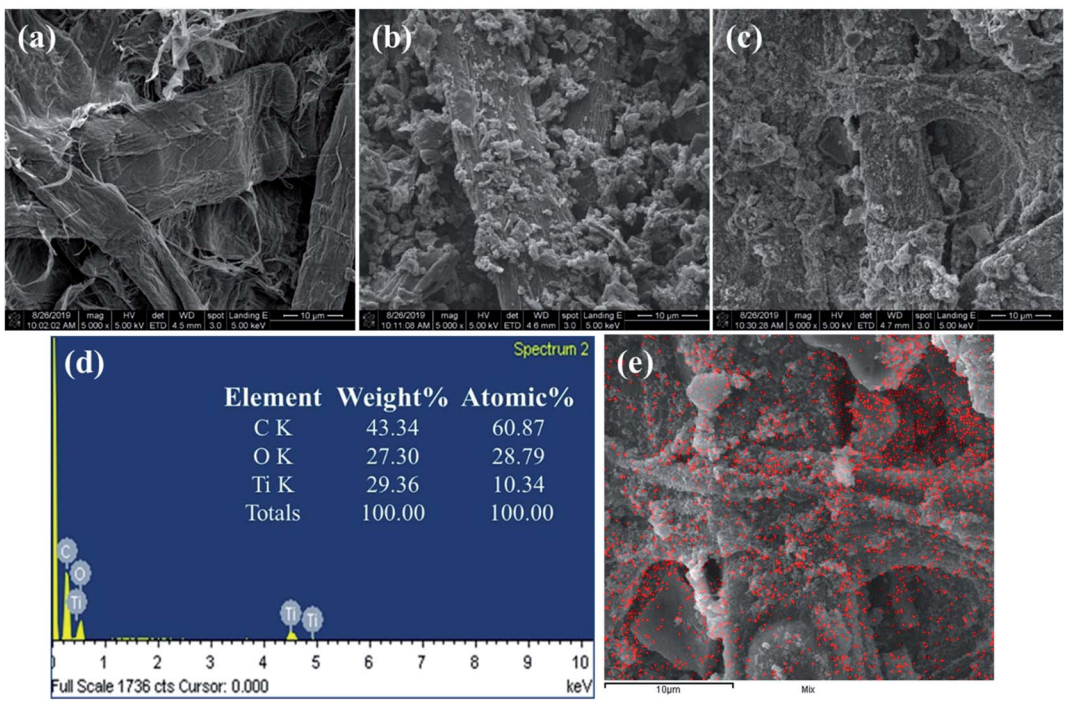

Fig. 2 SEM images of (a) pristine lens tissue, (b) lens tissue loaded with AC only and (c) lens tissue loaded with AC-P25. (d) EDS spectrum of AC-P25 and (e) EDS Ti elemental mapping of AC-P25.

3.2 Steam generation performance

The steam generation performances of systems with and without interfacial evaporation devices were compared by measuring the evaporation weight loss of water under illumination by simulated sunlight; the results are shown in Fig. 3. A larger weight loss indicates that more steam is generated. The evaporation rate (r_{evp}) under illumination was also acquired by calculating the slope of the weight loss curve; the calculation of r_{evp} at a given time t is explained in the ESI (Text S2†). Fig. 3(a) shows that AC-P25/foam generated the largest amount of steam in 45 min. In addition, in Fig. 3(b), the results show that PE foam not only improved the steam generation performance but also shortened the response time required to reach the steady-state r_{evp}. For those without interfacial evaporation (*i.e.*, submerged AC-P25 and water-only conditions), the steady-state values of evaporation rates were barely reached even after 45 min under illumination. However, for interfacial evaporation systems, the evaporation rates reached their steady-state values within approximately only 10 min. Furthermore, among the systems, AC-P25/foam showed the highest steam generation rate with r_{evp} (r_{evp} = 2.1 kg m^{-2} h^{-1}) approximately 3 times, 1.7 times and 1.3 times those under water-only (r_{evp} = 0.68 kg m^{-2} h^{-1}), submerged AC-P25 (r_{evp} = 1.23 kg m^{-2} h^{-1}) and graphite/foam conditions (r_{evp} = 1.61 kg m^{-2} h^{-1}) in 45 min, respectively. The superior steam generation performance of AC-P25/foam can be explained by the following two reasons. One reason is its better optical absorption in the UV to near infrared regions, further leading to efficient photothermal conversion, as described in detail as follows. The electrons in a carbon material can be activated from the ground-state orbital (HOMO) to a higher energy orbital (LUMO) when the incident light energy matches the electronic transition within the molecule. Subsequently, the excited electrons relax *via* electron–phonon coupling; thus, the absorbed energy is transferred to vibration modes in the atomic lattices, increasing the temperature of the material[2,27] and consequently facilitating water evaporation. The other reason may be the use of PE foam as the supporting layer; PE foam separated the evaporative portion of the water from the bulk water. Additionally, PE foam has a low thermal conductivity and can suppress heat loss to the bulk water, resulting in the heat localization phenomenon and making the evaporation process more efficient (this is further discussed and supported by the results in Fig. 4 in this section). Li *et al.*[28] used biochar-loaded filter paper to generate high-temperature steam for performing steam sterilization and found that effective sterilization and a shorter heat-up time were achieved through interfacial evaporation. On the other hand, notably, the steam generation experiments were conducted in a chamber of the solar simulator, which was similar to a closed system (Fig. S2†); thus, the

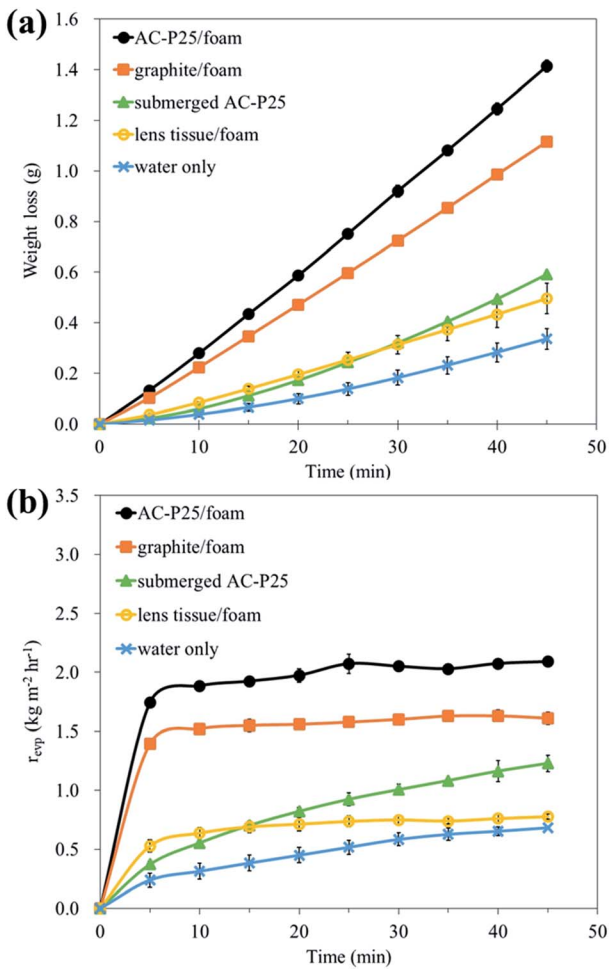

Fig. 3 (a) Weight loss and (b) evaporation rates of different systems under irradiation.

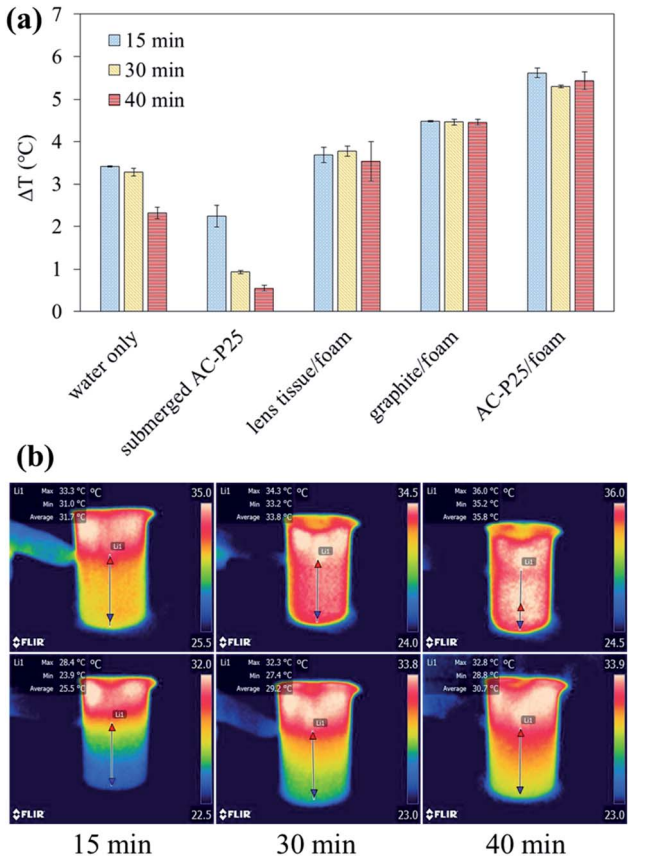

Fig. 4 (a) Temperature difference between the water surface and bottom and (b) IR images under irradiation: submerged AC-P25 (top) and AC-P25/foam (bottom).

ambient temperature in the chamber is easily increased under simulated sunlight illumination. Under this condition, the system may receive extra thermal energy from the warmer surrounding environment,[29,30] which also causes an increase in the evaporation rate of the system. However, compared with other systems studied in this work, the highest evaporation rate achieved by AC-P25/foam still indicated its promising performance as a solar steam generator.

To confirm the heat localization ability of interfacial evaporation, an IR camera was utilized to measure the temperature difference between the water surface and the bottom. The temperature differences in the different systems and IR images of the systems with submerged AC-P25 or AC-P25/foam are shown in Fig. 4; the detailed measured temperature values are provided in Table S2.† Fig. 4(a) shows that the temperature difference in the systems without interfacial evaporation gradually decreased with time, especially for submerged AC-P25. In contrast, when applying interfacial evaporation devices, the temperature difference remained nearly the same under illumination, indicating that interfacial evaporation can achieve heat localization. Taking the IR images of submerged AC-P25 and AC-P25/foam in Fig. 4(b) as an example, at 15 min of illumination, a temperature difference between the water surface and the bottom can be observed in both systems. After 30 min, the temperature distribution became uniform in the submerged AC-P25 system. However, for the AC-P25/foam system, a nonuniform temperature distribution can still be observed even after 40 min of illumination. Due to the suppression of the heat loss to the bulk water, the successful heat localization caused by PE foam reiterated the outstanding steam generation performance of AC-P25/foam. Accordingly, AC-P25/foam was chosen as the steam generation device in the following solar distillation experiments.

The reusability of AC-P25/foam was also examined by conducting a steam generation test under 45 min of illumination for 7 cycles to determine whether the evaporation performance will decrease after each cleaning process to remove salt crystals on the device surface. As shown in Fig. 5, the evaporation performance of the AC-P25/foam remained nearly unchanged within 7 cycles (the corresponding original mass change profile is provided in Fig. S4(a)†), indicating the stable performance of AC-P25/foam for steam generation. However, we observed that AC-P25 was slightly flaked after 7 cycles of the steam generation test (Fig. S5†). Future investigations on improving the stability and durability of the photothermal material are needed.

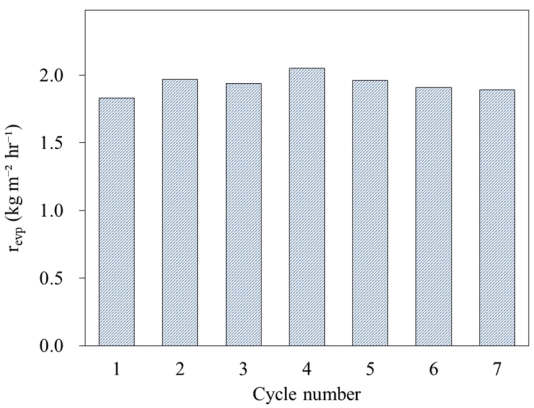

Fig. 5 Evaporation rates for seven cycles using AC-P25/foam.

3.2.1 Effect of suspended solids on steam generation. Since suspended solids commonly exist in environmental waters and industrial effluents, the reduction in the steam generation efficiency caused by the scattering effect of suspended solids is possible if these waters are used in the solar distillation process. To understand how suspended solids affect the evaporation performance in different systems, the influence of suspended solids (represented by kaolinite) on the submerged AC-P25 and interfacial AC-P25/foam systems was investigated. The results were compared by calculating the enhancement due to the different evaporation devices (*i.e.*, submerged AC-P25 and AC-P25/foam) according to eqn (1):

$$\Delta r_{evp} = r_{evp}\,(\text{with evaporation device}) - r_{evp}\,(\text{without evaporation device}) \quad (1)$$

where r_{evp} is the evaporation rate after 45 min of illumination by simulated sunlight. The results are shown in Fig. 6 (the corresponding original mass change profile is provided in Fig. S4(b)†). With increasing concentrations of kaolinite, the enhancement of the evaporation rate in the conventional solar evaporation system (*i.e.*, submerged AC-P25) decreased; however, for the interfacial evaporation system (*i.e.*, AC-P25/foam), the enhancement was less affected by the kaolinite in water. This is not surprising considering that AC-P25/foam absorbed the incident light slightly above the water surface, reducing the possibility of light scattering caused by the suspended solids in water. Notably, although the concentrations of suspended solids in this experiment were relatively high, the results still showed that the enhancement in the interfacial system was only slightly affected even under extremely high concentrations of suspended solids.

3.3 The multifunctional interfacial system: clean water generation, VOC removal and saline water desalination

In this section, the solar still system with AC-P25/foam inside was utilized to conduct the clean water generation experiment

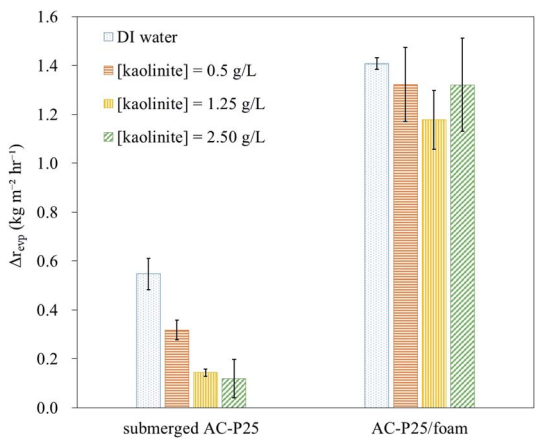

Fig. 6 Effect of suspended solids on evaporation after 45 min of irradiation.

both on a laboratory scale (by solar simulator) and under actual sunlight to understand the system applicability. The different water matrices, including VOC-containing water and synthetic saline water, were used as the source water; the solar still system design is introduced in Section 2.5.

A VOC-containing water matrix was used as source water to explore the possibility of distilled water collection with simultaneous VOC removal *via* the AC-P25/foam interfacial system in the solar still. To first understand the sorption/photocatalytic ability of the synthesized AC-P25, the phenol removal test was conducted using 10 mg L^{-1} phenol solution in a beaker with the temperature controlled at 20 °C in water bath, and an AC-P25 sheet (without PE foam) was placed at the bottom of the beaker, thereby fully submerging it in the phenol solution. The removal of phenol is shown in Fig. S6.† Phenol remained stable under direct sunlight photolysis, and nearly 40% was removed through pure adsorption with AC-P25. Moreover, under illumination, approximately 20% of phenol was further removed. Different trends of phenol removal in the dark and under illumination using AC-P25 can also be observed. The change in the trend of phenol removal under illumination implied the involvement of the photocatalytic process by the TiO_2 photocatalyst blended in the material. The TiO_2 photocatalytic reactions are described in eqn (2)–(4). During the photocatalytic reaction, when TiO_2 is irradiated with energetic light ($h\nu$ > 3.2 eV), an electron–hole pair is generated, further generating the strong hydroxyl radical (˙OH) oxidant. The ˙OH or valence hole (h_{VB}^+) in the system would react with the phenol pollutant and lead to its degradation.[31] Therefore, AC-P25 showed the ability to degrade phenol in the solution through a combination of adsorption and photocatalytic degradation.

$$TiO_2 + h\nu \rightarrow e^- + h_{VB}^+ \quad (2)$$

$$h_{VB}^+ + H_2O \rightarrow {}^{\cdot}OH + H^+ \quad (3)$$

$$^{\cdot}OH \text{ (or } h_{VB}^+) + \text{phenol} \rightarrow \text{degradation products} \quad (4)$$

After the ability of AC-P25 for phenol removal was substantiated, the solar distillation of a solution containing phenol was performed with the solar still. Fig. 7 shows the phenol concentrations in the initial phenol solution, phenol solution after solar distillation and distilled water in systems with or without AC-P25/foam. For the system without AC-P25/foam, the distilled water had almost the same concentration of phenol as the initial phenol solution; this indicated that after solar distillation, phenol was vaporized along with water and collected in the distilled water. However, with solar distillation using AC-P25/foam, phenol was significantly removed (~95%) and was detected at only trace levels (0.49 mg L^{-1}) in the distilled water. It is presumed that the phenol in the solution transported to the surface of the device came into direct contact with AC-P25, and phenol was continuously removed through adsorption and photocatalytic degradation during solar distillation. Therefore, this system shows the ability to prevent phenol enrichment in distilled water during solar distillation.

In addition to being able to prevent VOC enrichment, the desalination ability of the solar still system under real sunlight was also studied to evaluate the application potential of the system. For this experiment, synthetic saline water was utilized as the experimental solution to simulate the average salinity of seawater (3.5 wt%). Outdoor sunlight illumination experiments with and without AC-P25/foam were conducted in Taipei, Taiwan (25°01′03.8″N 121°32′36.1″E) in February, 2020. The solar flux density and the surface temperature of the AC-P25/foam were recorded; the data are shown in Fig. S7 and S8,†

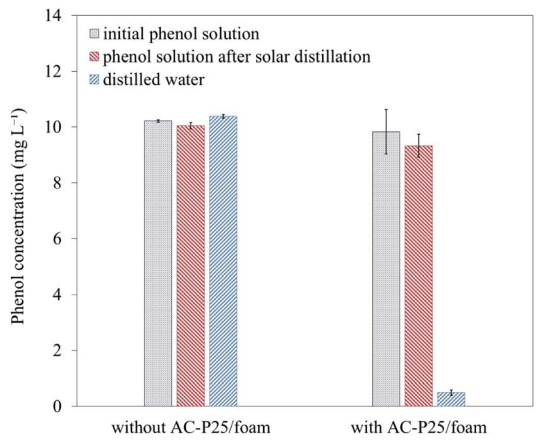

Fig. 7 Phenol concentration before and after solar distillation using the solar still system with or without AC-P25/foam.

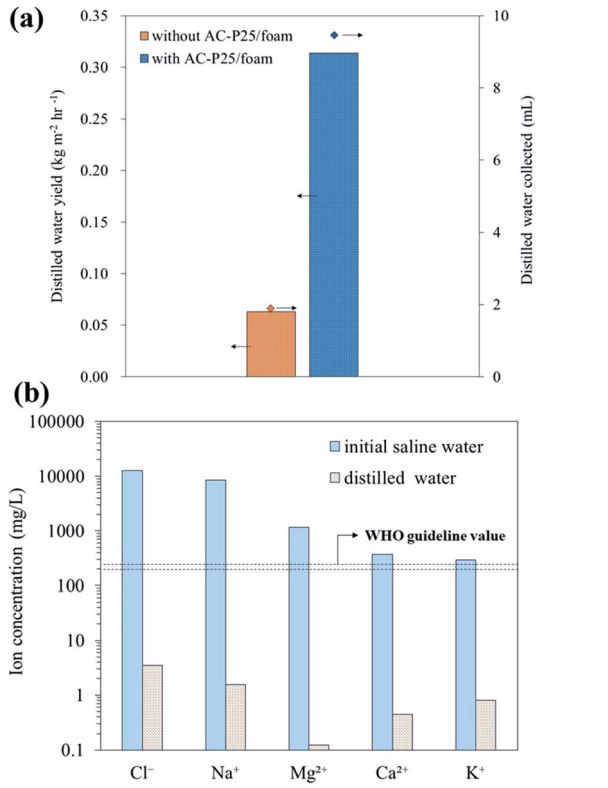

Fig. 8 (a) Distilled water production (bar graph: refers to the left *y*-axis; diamond symbol: refers to the right *y*-axis) and (b) desalination ability using the solar still system with AC-P25/foam under outdoor sunlight irradiation.

respectively. The distilled water was collected in the outer bowl after 6 h of solar irradiation from 09 : 30 to 15 : 30 on both days. In Fig. 8(a), under outdoor solar irradiation, solar distillation with AC-P25/foam reached a distilled water yield of 0.3138 kg m^{-2} h^{-1}, which was approximately 5 times that without the evaporation device (0.0628 kg m^{-2} h^{-1}); the collected volumes of the distilled water were 9.46 and 1.89 mL in the systems with and without AC-P25/foam, respectively. Comparing the distilled water production (Fig. 8(a)) with the evaporation rate (Fig. 3(b)) of the solar still systems shows that the AC-P25/foam device achieves a high evaporation rate, resulting in its high water production yield. Additionally, after the solar distillation process using AC-P25/foam, the Cl^- and Na^+ levels in the distilled water were 3.5 and 1.6 mg L^{-1} (Fig. 8(b)), respectively, which are well below the guideline value for drinking water established by the World Health Organization (200–250 mg L^{-1});[32] Mg^{2+}, Ca^{2+} and K^+ were also present in trace amounts in the distilled water (Mg^{2+} = 0.1 mg L^{-1}, Ca^{2+} = 0.4 mg L^{-1} and K^+ = 0.8 mg L^{-1}). Overall, the high distilled water productivity and acceptable water quality suggest the efficacy of solar distillation using interfacial evaporation devices for desalination.

4. Conclusion

An interfacial evaporation device with a high steam generation efficiency was successfully established by combining easily available materials, including AC, TiO_2 (P25), lens tissue and PE foam. AC-P25 showed excellent optical absorption from the UV to the near-infrared region and thus can generate more thermal energy to vaporize water film on the device surface. In addition, the low thermal conductivity of PE foam restricted the heat loss to the bulk water, which enabled efficient utilization of the thermal energy generated at the device surface. The high optical absorption of AC-P25 and the heat localization induced by PE foam together promote the steam generation performance and make AC-P25/foam a superior evaporation device, with an r_{evp} of 2.1 kg m^{-2} h^{-1} after 45 min of illumination. The AC-P25/foam interfacial evaporation device not only exhibited stable evaporation performance, even after several cycle tests, but also was less affected by suspended solids in the water. Apart from better steam generation performance, AC-P25 was also proven to have the ability to remove VOCs (phenol; ~95% removal efficiency) in water through adsorption and photocatalysis under illumination. Additionally, the results of the outdoor solar distillation experiment showed that the desalination ability of the fabricated AC-P25/foam device resulted in a distilled water quality that easily met the WHO drinking water guideline. Overall, the device, with promising abilities in water production, prevention of VOC enrichment and desalination, demonstrated great potential for use in solar distillation.

Conflicts of interest

There are no conflicts to declare.

Nomenclature

AC-P25:	Activated carbon combined with P25 TiO_2
PE:	Polyethylene
VOCs:	Volatile organic compounds
UV-vis-NIR:	Ultraviolet-visible-near infrared
FESEM:	Field emission scanning electron microscopy
EDS:	Energy dispersive spectrometry
HPLC-DAD:	High-performance liquid chromatography coupled with a diode-array detector
ICP-OES:	Inductively coupled plasma optical emission spectrometry
r_{evp}:	Evaporation rate (kg m^{-2} h^{-1})
Δr_{evp}:	r_{evp} (with an evaporation device) − r_{evp} (without an evaporation device) (kg m^{-2} h^{-1})
ΔT:	Temperature difference (°C)

Acknowledgements

This work was financially supported by Ministry of Science and Technology through the projects MOST 105-2628-E-002-002-MY3 and MOST 103-2221-E-002-240-MY5 and by National Taiwan University from Excellence Research Program-Core Consortiums (NTU-CC-108L891305) within the framework of the Higher Education Sprout Project by the Ministry of Education in Taiwan.

References

1 A. J. D. Michaels, Membranes, membrane processes, and their applications: needs, unsolved problems, and challenges of the 1990's, *Desalination*, 1990, **77**, 5–34.
2 M. Gao, L. Zhu, C. K. Peh, G. W. J. E. Ho and E. Science, Solar absorber material and system designs for photothermal water vaporization towards clean water and energy production, *Energy Environ. Sci.*, 2019, **12**, 841–864.
3 S. Yadav and K. Sudhakar, Different domestic designs of solar stills: a review, *Renewable Sustainable Energy Rev.*, 2015, **47**, 718–731.
4 M. K. Phadatare and S. K. Verma, Influence of water depth on internal heat and mass transfer in a plastic solar still, *Desalination*, 2007, **217**, 267–275.
5 S. Shanmugan, P. Rajamohan and D. Mutharasu, Performance study on an acrylic mirror boosted solar distillation unit utilizing seawater, *Desalination*, 2008, **230**, 281–287.
6 Y. Taamneh and M. Taamneh, Performance of pyramid-shaped solar still: experimental study, *Desalination*, 2012, **291**, 65–68.
7 T. Arunkumar, R. Jayaprakash, D. Denkenberger, A. Ahsan, M. S. Okundamiya, S. kumar, H. Tanaka and H. Ş. Aybar, An experimental study on a hemispherical solar still, *Desalination*, 2012, **286**, 342–348.
8 B. I. Ismail, Design and performance of a transportable hemispherical solar still, *Renewable Energy*, 2009, **34**, 145–150.
9 H. Ghasemi, G. Ni, A. M. Marconnet, J. Loomis, S. Yerci, N. Miljkovic and G. Chen, Solar steam generation by heat localization, *Nat. Commun.*, 2014, **5**, 4449.

10 D. Hao, Y. Yang, B. Xu and Z. Cai, Efficient Solar Water Vapor Generation Enabled by Water-Absorbing Polypyrrole Coated Cotton Fabric with Enhanced Heat Localization, *Appl. Therm. Eng.*, 2018, **141**, 406–412.

11 L. L. Zhu, M. M. Gao, C. K. N. Peh and G. W. Ho, Recent progress in solar-driven interfacial water evaporation: Advanced designs and applications, *Nano Energy*, 2019, **57**, 507–518.

12 M. Gao, P. K. N. Connor and G. W. Ho, Plasmonic photothermic directed broadband sunlight harnessing for seawater catalysis and desalination, *Energy Environ. Sci.*, 2016, **9**, 3151–3160.

13 H. R. Li, Y. R. He, Y. W. Hu and X. Z. Wang, Commercially Available Activated Carbon Fiber Felt Enables Efficient Solar Steam Generation, *ACS Appl. Mater. Interfaces*, 2018, **10**, 9362–9368.

14 L. Chen, H. Y. Wang, S. Kuravi, K. Kota, Y. H. Park and P. Xu, Low-cost and reusable carbon black based solar evaporator for effective water desalination, *Desalination*, 2020, **483**, 114412.

15 M. M. Gao, L. L. Zhu, C. K. Peh and G. W. Ho, Solar absorber material and system designs for photothermal water vaporization towards clean water and energy production, *Energy Environ. Sci.*, 2019, **12**, 841–864.

16 S. L. Wu, H. L. Chen, H. L. Wang, X. L. Chen, H. C. Yang and S. B. Darling, Solar-driven evaporators for water treatment: challenges and opportunities, *Environ. Sci.: Water Res. Technol.*, 2021, **7**, 24–39.

17 P. Wang, Emerging investigator series: the rise of nano-enabled photothermal materials for water evaporation and clean water production by sunlight, *Environ. Sci.: Nano*, 2018, **5**, 1078–1089.

18 L. Shi, Y. Shi, S. Zhuo, C. Zhang, Y. Aldrees, S. Aleid and P. Wang, Multi-functional 3D honeycomb ceramic plate for clean water production by heterogeneous photo-Fenton reaction and solar-driven water evaporation, *Nano Energy*, 2019, **60**, 222–230.

19 J. Lou, Y. Liu, Z. Wang, D. Zhao, C. Song, J. Wu, N. Dasgupta, W. Zhang, D. Zhang, P. Tao, W. Shang and T. Deng, Bioinspired Multifunctional Paper-Based rGO Composites for Solar-Driven Clean Water Generation, *ACS Appl. Mater. Interfaces*, 2016, **8**, 14628–14636.

20 X. Liu, H. Cheng, Z. Guo, Q. Zhan, J. Qian and X. Wang, Bifunctional, Moth-Eye-Like Nanostructured Black Titania Nanocomposites for Solar-Driven Clean Water Generation, *ACS Appl. Mater. Interfaces*, 2018, **10**, 39661–39669.

21 R. Zhao, J. Xu, P. Tao, F. Shi, F. Yu, X. Zeng, C. Song, J. Wu, W. Shang and T. Deng, Clean water generation with switchable dispersion of multifunctional Fe_3O_4-reduced graphene oxide particles, *Prog. Nat. Sci.: Mater. Int.*, 2018, **28**, 422–429.

22 L. Shi, Y. Shi, S. F. Zhuo, C. L. Zhang, Y. Aldrees, S. Aleid and P. Wang, Multi-functional 3D honeycomb ceramic plate for clean water production by heterogeneous photo-Fenton reaction and solar-driven water evaporation, *Nano Energy*, 2019, **60**, 222–230.

23 C. J. Song, D. P. Qi, Y. Han, Y. Xu, H. B. Xu, S. J. You, W. Wang, C. Wang, Y. Wei and J. Ma, Volatile-Organic-Compound-Intercepting Solar Distillation Enabled by a Photothermal/Photocatalytic Nanofibrous Membrane with Dual-Scale Pores, *Environ. Sci. Technol.*, 2020, **54**, 9025–9033.

24 P.-F. Liu, L. Miao, Z. Deng, J. Zhou, H. Su, L. Sun, S. Tanemura, W. Cao, F. Jiang and L. Zhao, A mimetic transpiration system for record high conversion efficiency in solar steam generator under one-sun, *Mater. Today Energy*, 2018, **8**, 166–173.

25 H. M. M. Ibrahim, Photocatalytic degradation of methylene blue and inactivation of pathogenic bacteria using silver nanoparticles modified titanium dioxide thin films, *World J. Microbiol. Biotechnol.*, 2015, **31**, 1049–1060.

26 K. Sirirerkratana, P. Kemacheevakul and S. Chuangchote, Color removal from wastewater by photocatalytic process using titanium dioxide-coated glass, ceramic tile, and stainless steel sheets, *J. Cleaner Prod.*, 2019, **215**, 123–130.

27 J. R. Velez-Cordero and J. Hernandez-Cordero, Heat generation and conduction in PDMS-carbon nanoparticle membranes irradiated with optical fibers, *Int. J. Therm. Sci.*, 2015, **96**, 12–22.

28 J. Li, M. Du, G. Lv, L. Zhou, X. Li, L. Bertoluzzi, C. Liu, S. Zhu and J. Zhu, Interfacial Solar Steam Generation Enables Fast-Responsive, Energy-Efficient, and Low-Cost Off-Grid Sterilization, *Adv. Mater.*, 2018, **30**, 1805159.

29 H. M. Song, Y. H. Liu, Z. J. Liu, M. H. Singer, C. Y. Li, A. R. Cheney, D. X. Ji, L. Zhou, N. Zhang, X. Zeng, Z. M. Bei, Z. F. Yu, S. H. Jiang and Q. Q. Gan, Cold Vapor Generation beyond the Input Solar Energy Limit, *Adv. Sci.*, 2018, **5**, 1800222.

30 X. Q. Li, J. L. Li, J. Y. Lu, N. Xu, C. L. Chen, X. Z. Min, B. Zhu, H. X. Li, L. Zhou, S. N. Zhu, T. J. Zhang and J. Zhu, Enhancement of Interfacial Solar Vapor Generation by Environmental Energy, *Joule*, 2018, **2**, 1331–1338.

31 S. Ahmed, M. G. Rasul, W. N. Martens, R. Brown and M. A. Hashib, Heterogeneous photocatalytic degradation of phenols in wastewater: a review on current status and developments, *Desalination*, 2010, **261**, 3–18.

32 WHO, *Guidelines for drinking-water quality*, World Health Organization, 4th edn, 2011.